Self-consistent analysis of the hot spot dynamics for inertial confinement fusion capsules

J. Sanz
ETSI Aeronàuticos, Universidad Politécnica de Madrid, 28040 Madrid, Spain

J. Garnier
Laboratoire de Probabilités et Modèles Aléatoires & Laboratoire Jacques-Louis Lions, Université Paris VII, 2 Place Jussieu, 75251 Paris Cedex 5, France

C. Cherfils, B. Canaud, and L. Masse
Commissariat à l'Energie Atomique, Direction des Applications Militaires, Boîte Postale 12, 91680 Bruyères-le-Châtel, France

M. Temporal
ETSI Industriales, Universidad de Castilla-La Mancha, 13071 Ciudad Real, Spain

(Received 25 July 2005; accepted 6 October 2005; published online 11 November 2005)

In the context of the French Laser-Mégajoule fusion-research program, the hydrodynamic stability of the baseline direct-drive target is investigated at the hot spot surface during the deceleration phase by means of modeling and simulations. Using the convergence of the flow towards a self-similar solution, a closed system of ordinary differential equations is derived for the main hydrodynamic variables. An exact linear stability analysis is performed to compute the Rayleigh-Taylor growths. All theoretical predictions are compared to one-dimensional and two-dimensional single-mode detailed numerical results. © *2005 American Institute of Physics*. [DOI: 10.1063/1.2130315]

I. INTRODUCTION

Hydrodynamic stability of inertial confinement fusion (ICF) capsules during the deceleration stage has been recently studied in numerous papers, particularly in the direct drive configuration. First, Betti and co-workers[1–3] have addressed theoretically the ablative stabilization of the Rayleigh-Taylor type instability occurring during the deceleration phase. They have proposed an analysis of the hot spot dynamics in the quasi-isobaric approach by the use of a self-similar solution. But they only used the planar Betti-Goncharov formula[4] with time-averaged hydrodynamic values to give a rough estimate of the linear growth rates. Improvements of this model and time derivation of the linearized problem have then been published in parallel by Garnier-Cherfils[5] and Sanz-Betti,[6] but the sharp-boundary model (SBM) approach chosen in these papers cannot predict the evolution of the low modes. Atzeni and Temporal[7] have published detailed simulations of the deceleration phase of an indirectly driven target, done with the two-dimensional (2D) Lagrangian code DUED.[8–10] They have shown a displacement of the maximum of the Lagrangian perturbation amplitude inside the hot spot and a reduction of the time-averaged Rayleigh-Taylor instability (RTI) growth rate compared to classical theory such as Takabe-Bodner formula.[11] This has been confirmed more explicitly in a recent work[12] where a direct drive target was considered. In this work, a time analysis of the RTI growth rate deduced from single-mode DUED calculations has shown the total discrepancy between the classical theory and the hydrodynamic calculation.

The present paper is based on these previous works and addresses an analytical description of the RTI during the deceleration phase. The first part is devoted to the one-dimensional (1D) modeling of this phase; the thorough analysis of the coupling between the hot spot and the shell represents the original contribution of this part. The theoretical predictions of this new model are compared to 1D numerical results of the baseline Laser Mégajoule (LMJ) direct-drive capsule[12] with a very good agreement. In the second part of the paper, a linear stability analysis is performed to compute the RTI growth for an arbitrary self-similar one-dimensional flow. This analysis takes into account the spatial 1D profiles inside the hot spot. It allows an accurate prediction of the low modes growth rates, compared to previous models[5,6] where a SBM approximation was used. This new theory is applied to the baseline LMJ direct-drive capsule, and comparisons with 2D numerical simulations are presented.

II. MODELING THE DECELERATION HYDRODYNAMICS

A. The three-dimensional hot spot model

The flow inside the hot spot is subsonic, which allows us to adopt the subsonic flow ordering. To lowest order we get the flat pressure approximation $p(t,\mathbf{r})=p_h(t)$. Then, the mass, momentum, and energy equations are

$$\partial_t(\rho)+\nabla\cdot(\rho\mathbf{u})=0, \tag{1}$$

$$\rho\partial_t\mathbf{u}+\mathbf{u}\cdot\nabla\mathbf{u}+\nabla p=0, \tag{2}$$

$$\partial_t p_h+\nabla\cdot(\gamma_h p_h\mathbf{u}-(\gamma_h-1)\kappa(T)\nabla T)=S, \tag{3}$$

where ρ is the density, $\mathbf{u}$ is the velocity flow, and p stands for the spatial fluctuations of the pressure. The momentum equation describes the fluctuations of the pressure and it can be

integrated *a posteriori*. $S=(\gamma_h-1)\rho^2 E_\alpha \theta\langle\sigma v\rangle/(4m_i^2)$ is the source term imposed by nuclear reaction, E_α is the α-particle energy, $\langle\sigma v\rangle$ is the fusion reaction rate, m_i is the ion mass. $\kappa(T)=\chi T^\nu$ is the Spitzer thermal conductivity. This system is completed by the standard ideal gas equation of state (EOS) $p_h=(\gamma_h-1)c_v\rho T$ with $\gamma_h=5/3$ for a monoatomic gas. c_v is the specific heat at constant volume. We approximate the fusion cross section by a quadratic form $\langle\sigma v\rangle\simeq S_\alpha T^2$. Such an approximation is valid as long as $6<T<20$ keV, which is the range relevant to ignition in ICF.[2] The local deposition approximation used here is strictly valid when all the α particles are absorbed within the hot spot. We artificially include the effect of α-particle diffusion by adding a multiplicative factor $\theta\leqslant 1$ to the α-power term.

As shown in Refs. 1–3 and 6, Eq. (3) can be integrated over the hot spot volume V_h enclosed by the shell inner surface where the shell material is cold and the heat flux can be neglected, leading to

$$\frac{\mu_\alpha p_h^2-\dot{p}_h}{p_h}=\gamma_h\frac{\dot{V}_h}{V_h}, \tag{4}$$

where the dot stands for a time-derivative. The analysis of Eqs. (2) and (3) is performed in the following way. First, we locally integrate Eq. (3), and we express the velocity in the hot region as

$$\mathbf{u}=\frac{\bar{\chi}T^\nu}{\gamma_h p_h}\nabla T+\frac{\mathbf{r}}{3\gamma_h}\left(\mu_\alpha p_h-\frac{\dot{p}_h}{p_h}\right)+\mathbf{u}_{\rm rot},\qquad \nabla\cdot\mathbf{u}_{\rm rot}=0, \tag{5}$$

where $\bar{\chi}=(\gamma_h-1)\chi$ and $\mu_\alpha=E_\alpha S_\alpha/[4(\gamma_h-1)m_i^2c_v^2]$. $\mathbf{u}_{\rm rot}$ is the rotational part of the velocity $\mathbf{u}$. The rotational component $\mathbf{u}_{\rm rot}$ is induced by the vorticity $\nabla\times\mathbf{u}_{\rm rot}$ convected to the hot spot from the ablation front and also generated in the hot spot region by the baroclinic effect $\nabla\rho\times\nabla p$. Then, substituting this expression for the velocity into the mass equation (1), and eliminating the density by the EOS, we get the equation governing the evolution of the temperature:

$$[\dot{p}_h(\gamma_h-1)+\mu_\alpha p_h^2]T-\gamma_h p_h\partial_t T-\left[\frac{\mathbf{r}}{3}(\mu_\alpha p_h^2-\dot{p}_h)+\gamma_h p_h\mathbf{u}_{\rm rot}\right]\cdot\nabla T+\frac{\bar{\chi}}{\nu}T^2\Delta(T^\nu)=0. \tag{6}$$

The system of equations (1)–(6) is used in the next section to determine the structure of the unperturbed self-similar flow in spherical geometry, and it will be used in Sec. III A 2 to study the structure of the flow in the hot spot when it is perturbed with respect to the self-similar solution.

B. The hot spot model in spherical geometry

A detailed analysis of the flow can be performed if we assume spherical geometry. This analysis provides complete information for the unperturbed flow that will be used in Sec. III A 2 where the Rayleigh-Taylor instability growths are studied.

A multi-scale analysis of the hot spot during the deceleration phase is an efficient way to obtain information at a macroscopic scale, useful for the determination of ignition criteria, and at a microscopic scale, necessary for the computations of RTI growth rates. Theoretical studies have been performed in different papers.[2,3,5] It is shown that the flow inside the hot spot converges toward a self-similar profile whose dynamics depends on the hot spot uniform pressure. Besides, it is demonstrated that the hot spot is separated from the shell by a thin layer that also possesses a microscopic self-similar profile. Finally, the derivation of a closed system for the main physical quantities requires the coupling of the flows inside the hot spot and in the shell.

1. The self-similar flow in the hot spot

In this paragraph we report the main results obtained in Refs. 2, 3, 5, and 6 describing the structure of the self-similar flow inside the hot spot. In spherical geometry Eq. (4) can be written in terms of the hot spot radius R_h as

$$\frac{\mu_\alpha p_h^2-\dot{p}_h}{p_h}=3\gamma\frac{\dot{R}_h}{R_h}. \tag{7}$$

Let us seek a self-similar form for the temperature profile

$$T(t,r)=T_0\left(t,\frac{r}{R_h(t)}\right),\quad T_0(t,\eta)=T_h(t)\psi_0^{1/\nu}(\eta),$$

with $T_h(t)=T(t,r=0)$ the central hot spot temperature. Substituting this ansatz into Eq. (6) we get the compatibility equation: $\forall\,\eta\in[0,1]$, $\forall t\geqslant 0$,

$$[\eta\partial_\eta\psi_0(\eta)+2\partial_\eta\psi_0(\eta)]\left[\frac{\bar{\chi}T_h^{\nu+2}}{\gamma R_h^2}\right](t)+[\eta\psi_0^{-1/\nu}(\eta)]\times\left[\nu T_h p\frac{\dot{M}_h}{M_h}\right](t)=0,$$

with $M_h(t)$ the hot spot mass. The compatibility equation admits a solution if

$$\frac{\dot{M}_h(t)}{M_h(t)}=\frac{\bar{\chi}T_h^{\nu+1}(t)}{\nu a_\nu\gamma R_h^2(t)p_h(t)} \tag{8}$$

for a constant a_ν that also parametrizes the equation satisfied by ψ_0:

$$a_\nu\partial_\eta(\eta^2\partial_\eta\psi_0)+\eta^2\psi_0^{-1/\nu}=0, \tag{9}$$

with the boundary conditions: $\psi_0(0)=1$, $\partial_\eta\psi_0(0)=0$. The temperature becomes evanescent at the edge of the hot spot, $\eta=1$, so that $\psi_0(1)=0$. For any given $\nu>1$, these conditions are fulfilled only for a particular value of a_ν ($a_{\nu=5/2}\simeq 0.197$). Substituting into Eq. (5), we get the unperturbed velocity profile

$$u(t,r)=u_0\left(t,\frac{r}{R_h(t)}\right),\qquad u_0(t,\eta)=\dot{R}_h(t)\eta+V_b(t)a_\nu[\psi_0^{1/\nu}\partial_\eta\psi_0](\eta), \tag{10}$$

$$V_b(t) = R_h(t)\frac{\dot{M}_h(t)}{M_h(t)}. \tag{11}$$

The isobaric approximation gives the density profile $\rho(t,r) = \rho_h(t)\psi_0^{-1/\nu}(r/R_h(t))$, where $\rho_h(t)$ is the central hot spot density. As a result the mass ablation rate at the edge of the hot spot (toward the hot spot) is

$$\dot{m}_0(t) = \rho_h(t)V_b(t)a_\nu|\partial_\eta\psi_0(1)|, \tag{12}$$

where $\partial_\eta\psi_0(1)$ depends only on ν ($\partial_\eta\psi_0(1)\simeq -2.96$ if $\nu = 5/2$). Finally, the fluctuations of the pressure field can be obtained from Eq. (2):

$$p(t,r) = p_0\left(t, \frac{r}{R_h(t)}\right),$$
$$\partial_\eta p_0(t,\eta) = -\rho_h(t)\psi_0^{-1/\nu}(\eta)[R_h\partial_t u_0 + (u_0 - \eta\dot{R}_h)\partial_\eta u_0]. \tag{13}$$

This analysis shows that all hydrodynamic quantities and profiles can be computed in terms of the hot spot pressure $p_h(t)$. This pressure will be determined by closing the system with a shell model for the region $r > R_h$.

2. A refined thick shell model

A thick shell model originally proposed by Betti *et al.*[3] can be used to derive a closed system of ordinary differential equations governing the evolutions of the characteristic parameters of the hot spot and the shell.[5] In this section we present a refined and extended version of this model. In the previous versions the velocity profile in the shell at the beginning of the deceleration phase was assumed to be uniform and given by the implosion velocity. However simulations have shown that this hypothesis is not fulfilled, so we have extended the model to take into account arbitrary initial spatial profiles for the density inside the shell and affine profiles for the velocity inside the shell. This generalization is not straightforward as the number of degrees of freedom is increased, which makes the derivation of a closed system more tricky. We could push forward the extension to take into account an arbitrary initial velocity profile, but this would lead to unnecessary complications. Indeed our refined model is both mathematically tractable and physically relevant, and it turns out to provide theoretical predictions in good agreement with numerical results as we shall see below.

The thick shell model takes into account the return shock in the cold unperturbed shell. The deceleration phase actually starts when the shock reflected from the center of the capsule interacts with the incoming shell. We thus consider that the shock starts at time 0 from the edge of the hot spot and propagates within the shell. We denote by R_h the hot spot radius and by R_s the shock position. Three regions can be distinguished:

(1) $r < R_h(t)$ corresponds to the hot spot.
(2) $R_h(t) < r < R_s(t)$ corresponds to the shocked shell.
(3) $r > R_s(t)$ corresponds to the cold unperturbed shell, whose pressure is much lower.

Let us first consider the outer region $r > R_s(t)$. The shell is in free-fall conditions with an evanescent pressure and the flow is supersonic. At time 0, the density profile is ρ_0 and the velocity profile u_0. The density profile can be arbitrary, but we assume that the velocity profile is affine:

$$\rho_0(r) = \frac{M_{\rm sh}}{4\pi r^2\Delta_0}\bar{\rho}_0\left(\frac{r-R_0}{\Delta_0}\right), \tag{14}$$

$$u_0(r) = -V_i\left(1 - \eta_0\frac{r-R_0}{\Delta_0}\right), \tag{15}$$

where V_i is the implosion velocity, $M_{\rm sh}$ is the initial shell mass, R_0 is the initial inner radius of the shell (i.e., the initial position of the shock or the initial radius of the hot spot), Δ_0 is the initial thickness of the shell. The normalized profile $\bar{\rho}_0$ is such that $\bar{\rho}_0(x) = 0$ for $x \leqslant 0$, $\bar{\rho}_0(x) > 0$ for $x > 0$, and $\int_0^\infty \bar{\rho}_0(x)dx = 1$. The parameter η_0 models the non-uniformity of the velocity profile inside the shell. By neglecting heat flow and nuclear reactions inside the free-fall shell, it is possible to solve the Euler equations and to get that, for $r > R_s(t)$,

$$u_{\rm ff}(t,r) = -V_i\frac{1 - \eta_0\dfrac{r-R_0}{\Delta_0}}{1 + \eta_0\dfrac{V_i t}{\Delta_0}}, \tag{16}$$

$$\rho_{\rm ff}(t,r) = \frac{M_{\rm sh}}{4\pi r^2\Delta_0\left(1 + \eta_0\dfrac{V_i t}{\Delta_0}\right)}\bar{\rho}_0\left(\frac{r + V_i t - R_0}{\Delta_0\left(1 + \eta_0\dfrac{V_i t}{\Delta_0}\right)}\right). \tag{17}$$

We denote by $M_{\rm ss}$ the shocked shell mass and $U_h = \dot{R}_h$. Using the same method as in Ref. 5 we derive the following closed system of ordinary differential equations for the five variables $(R_s, R_h, U_h, M_{\rm ss}, p_h)$:

$$\dot{R}_s = -\frac{\gamma_s - 1}{2}u_{\rm ff}(t,R_s) + \frac{\gamma_s + 1}{2}\left\{U_h + \left[\left(3\frac{\gamma_h}{\gamma_s} - 2\right)\frac{U_h}{R_h} - \frac{\mu_\alpha}{\gamma_s}p_h\right][R_s - R_h]\right\}, \tag{18}$$

$$\dot{R}_h = U_h, \tag{19}$$

$$\dot{U}_h = \frac{R_h}{R_h\left(2 - \dfrac{3\gamma_h}{2\gamma_s}\right) + R_s\left(\dfrac{3\gamma_h}{2\gamma_s} - 1\right)}\left\{\left(1 - \frac{3\gamma_h}{2\gamma_s}\right)\times U_h\frac{\dot{R}_s R_h - R_s U_h}{R_h^2} + \frac{\mu_\alpha}{2\gamma_s}(\dot{p}_h(R_s - R_h) + p_h(\dot{R}_s - U_h)) + \frac{4\pi R_h^2 p_h}{M_{\rm ss}} - \frac{\dot{M}_{\rm ss}}{M_{\rm ss}}\left[U_h - u_{\rm ff}(R_s,t) + \left(\left(\frac{3\gamma_h}{2\gamma_s} - 1\right)\frac{U_h}{R_h} - \frac{\mu_\alpha}{2\gamma_s}p_h\right)(R_s - R_h)\right]\right\}, \tag{20}$$

$$\dot{M}_{\rm ss} = 4\pi R_s^2\rho_{\rm ff}(t,R_s)[\dot{R}_s - u_{\rm ff}(t,R_s)], \tag{21}$$

$$\dot{p}_h = -3\gamma_h \frac{U_h}{R_h} p_h + \mu_\alpha p_h. \tag{22}$$

The initial conditions are $R_s(0)=R_0$, $R_h(0)=R_0$, $U_h(0)=0$, $M_{ss}(0)=0$, $p_h(0)=p_0$. The adiabatic exponent is γ_h in the hot spot and γ_s in the shell. This system can be closed by the choice of the model for the flow in the free-fall shell. From now on we take the model (16) and (17) and we consider the dimensionless variables

$$\bar{R}_s = \frac{R_s}{R_0}, \quad \bar{R}_h = \frac{R_h}{R_0}, \quad \bar{U}_h = \frac{U_h}{V_i}, \quad \bar{p}_h = \frac{p_h}{p_0},$$

$$\bar{M}_{ss} = \frac{M_{ss}}{M_{sh}}, \quad \tau = \frac{V_i t}{R_0}.$$

The system can be reduced to

$$\bar{R}_s' = \frac{\gamma_s - 1}{2} \frac{1 - \eta_0 A_0 (\bar{R}_s - 1)}{1 + \eta_0 A_0 \tau} + \frac{\gamma_s + 1}{2} \times \left\{ \bar{U}_h + \left[\left(3\frac{\gamma_h}{\gamma_s} - 2 \right) \frac{\bar{U}_h}{\bar{R}_h} - \frac{Y_\alpha}{\gamma_s \hat{\epsilon}_0^2} \bar{p}_h \right] [\bar{R}_s - \bar{R}_h] \right\}, \tag{23}$$

$$\bar{R}_h' = \bar{U}_h, \tag{24}$$

$$\bar{U}_h' = \frac{\bar{R}_h}{\bar{R}_h \left(2 - \frac{3\gamma_h}{2\gamma_s} \right) + \bar{R}_s \left(\frac{3\gamma_h}{2\gamma_s} - 1 \right)} \left\{ \left(1 - \frac{3\gamma_h}{2\gamma_s} \right) \times \bar{U}_h \frac{\bar{R}_s' \bar{R}_h - \bar{R}_s \bar{U}_h}{\bar{R}_h^2} + \frac{Y_\alpha}{2\gamma_s \hat{\epsilon}_0^2} (\bar{p}_h' (\bar{R}_s - \bar{R}_h) + \bar{p}_h (\bar{R}_s' - \bar{U}_h)) + \frac{1}{\hat{\epsilon}_0} \frac{\bar{R}_h^2 \bar{p}_h}{\bar{M}_{ss}} - \frac{\bar{M}_{ss}'}{\bar{M}_{ss}} \times \left[\bar{U}_h + \frac{1 - \eta_0 A_0 (\bar{R}_s - 1)}{1 + \eta_0 A_0 \tau} + \left(\left(\frac{3\gamma_h}{2\gamma_s} - 1 \right) \frac{\bar{U}_h}{\bar{R}_h} - \frac{Y_\alpha}{2\gamma_s \hat{\epsilon}_0^2} \bar{p}_h \right) (\bar{R}_s - \bar{R}_h) \right] \right\}, \tag{25}$$

$$\bar{M}_{ss}' = \frac{A_0}{1 + \eta_0 A_0 \tau} \left(\frac{1 - \eta_0 A_0 (\bar{R}_s - 1)}{1 + \eta_0 A_0 \tau} + \bar{R}_s' \right) \times \bar{\rho}_0 \left(A_0 \frac{\bar{R}_s + \tau - 1}{1 + \eta_0 A_0 \tau} \right), \tag{26}$$

$$\bar{p}_h' = -3\gamma_h \frac{\bar{U}_h}{\bar{R}_h} \bar{p}_h + \frac{Y_\alpha}{\hat{\epsilon}_0^2} \bar{p}_h, \tag{27}$$

with the initial conditions $\bar{R}_s(0)=1$, $\bar{R}_h(0)=1$, $\bar{U}_h(0)=0$, $\bar{M}_{ss}(0)=0$, and $\bar{p}_h(0)=1$. Here the primes stand for derivatives with respect to τ. The four main free parameters of the problem are

$$\hat{\epsilon}_0 = \frac{M_{sh} V_i^2}{4\pi p_0 R_0^3}, \quad Y_\alpha = \frac{\mu_\alpha p_0 R_0}{V_i} \hat{\epsilon}_0^2, \quad A_0 = \frac{R_0}{\Delta_0}, \quad \eta_0.$$

Several features deserve some comments.

a. Dependence with respect to the conductivity law. The system of five differential equations allows us to obtain the hot spot pressure and radius. It is interesting to notice that it does not depend on the values of the coefficient χ and the Spitzer exponent ν. All that is required is that the temperature inside the hot spot is much higher than the temperature inside the shell. A very precise description of the internal dynamics of the shocked shell is not required, because only averaged quantities (such as the shocked shell mass or the average shocked shell velocity) are necessary to get a closed system. However, it is important to have rather good estimates of the initial spatial profiles of the shell density and velocity. Besides, it is crucial to have the correct equations of state in the hot spot and in the shell. In particular, it is important to take into account the existence of two adiabatic exponents in the shell and in the hot spot.

The exact values of the coefficient χ and the exponent ν are necessary to derive the expression of the hot spot mass

$$M_h(t) = \left[M_h(0)^{\nu+1} + c_1 c_v^{-\nu-1} (\gamma_h - 1) \times \chi (R_h(0)^{3\gamma_h} p_h(0))^{(3\nu+1)/(3\gamma_h)} \times \int_0^t p_h(s)^{[3(\gamma_h-1)\nu-1]/(3\gamma_h)} \times \exp\left(\frac{(3\nu+1)\mu_\alpha}{3\gamma_h} \int_0^s p_h(\tau) d\tau \right) ds \right]^{1/(\nu+1)}. \tag{28}$$

The coefficient c_1 only depends on the exponent ν and the adiabatic exponent γ_h,

$$c_1 = \frac{(\nu+1) m_\nu^{\nu+1}}{\nu a_\nu \gamma_h (\gamma_h - 1)^{\nu+1}},$$

with

$$m_\nu = 4\pi \int_0^1 \psi_0^{-1/\nu}(\eta) \eta^2 d\eta. \tag{29}$$

For $\nu=5/2$ and $\gamma_h=5/3$ we have $m_{\nu=5/2} \simeq 7.33$ and $c_1 \simeq 1.88 \times 10^4$. The mass flow $\dot{m}_0$ can then be deduced by the formula

$$\dot{m}_0(t) = \frac{\dot{M}_h(t)}{4\pi R_h^2(t)}.$$

The central hot spot density $\rho_h(t)$ can be computed from the hot spot mass $M_h(t)$ and the theoretical self-similar density profile $\rho_h(t) \psi_0^{-1/\nu}(r/R_h(t))$. The relationship between the hot spot mass and the central hot spot density depends only on the Spitzer exponent through the formula

$$\rho_h(t) = \frac{M_h(t)}{m_\nu R_h(t)^3}.$$

b. Determination of the shell density and ablation velocity. To obtain the shell density $\rho_{sh}(t)$ and the ablation velocity

$V_a(t)$, a good description of the shocked shell is required. The so-called shell density is defined as the density at the shell inner surface. It may be different from the maximal shell density because the spatial density profile inside the shell is not uniform. The strategy is to compute the shell density first, and then to deduce the ablation velocity from the identity $\dot{m}_0(t)=\rho_{\rm sh}(t)V_a(t)$. Up to now, only averaged quantities inside the shocked shell were required, while spatial profiles are now needed.

Note that the hot spot model is devoted to the predictions of the hot spot radius, pressure, and mass. It can yield the mass flow because the ablated mass flow is imposed by the heat flow from the hot spot toward the shell inner surface. However, the hot spot model is not primarily designed to describe the shell density, which depends on the precise choice of the shell model. A rigorous analysis would require one to solve the Euler equations in the shocked shell. However, an alternative procedure allows us to get a reasonable estimate of the shell density.

The isobaric approximation is not valid in the shocked shell. Actually, the flow is neither subsonic as it is in the hot spot, nor supersonic as it is in the free-fall shell. However, heat flow and nuclear reaction can be safely neglected, so that the energy conservation acquires a simple form. We assume that the shocked shell is a polytropic gas of EOS $p=(\gamma_s-1)\rho\epsilon$ with an adiabatic exponent $\gamma_s=7/4$. The choice of this EOS comes from observations by Herrmann[13] and Saillard[14] that the behavior of deuterium-tritium in the dense shell for the SESAME EOS[15] is well described with the value $\gamma_s=7/4$. In these conditions, the mass, momentum, and energy conservation equations can be written in spherical geometry as

$$\partial_t\rho+u\partial_r\rho+\frac{\rho}{r^2}\partial_r(r^2u)=0,$$

$$\partial_t u+u\partial_r u+\frac{1}{\rho}\partial_r p=0,$$

$$\partial_t p+u\partial_r p+\frac{\gamma_s p}{r^2}\partial_r(r^2u)=0.$$

The multi-scale analysis of the hot spot shows that, at the hot spot edge $r=R_h(t)$, the fluid velocity is almost the one of the interface $u(t,R_h(t))=\dot{R}_h(t)$. If we denote the shell density by $\rho_{\rm sh}(t):=\rho(t,r=R_h(t)^+)$, then the mass conservation equation at $R_h(t)$ gives

$$\dot{\rho}_{\rm sh}=\partial_t\rho+\dot{R}_h\partial_r\rho=(\dot{R}_h-u(t,R_h(t)))\ \partial_r\rho-\frac{\rho_{\rm sh}}{R_h^2}\partial_r(r^2u)\bigg|_{r=R_h^+}$$

By introducing $\alpha(t)=\partial_r u(t,r)|_{r=R_h(t)^+}+2\dot{R}_h/R_h$, we have $\dot{\rho}_{\rm sh}(t)=-\alpha(t)\rho_{\rm sh}(t)$. On the other hand, the energy conservation equation expressed at $r=R_h$ gives $\dot{p}_h(t)=-\gamma_s\alpha(t)p_h(t)$, which establishes a relation between the shell density $\rho_{\rm sh}$ and the pressure p_h at the edge of the hot spot (which is known from the integration of the system of differential equations (23)–(27):

$$\rho_{\rm sh}(t)p_h^{-1/\gamma_s}(t)=\text{constant}. \tag{30}$$

This equation can be used to obtain the shell density $\rho_{\rm sh}$, which in turn yields the ablation velocity V_a.

The above calculations can be pushed forward to obtain pieces of information about the spatial profiles of the density, velocity, and pressure inside the shocked shell. We have obtained the gradient of the velocity field at the shell inner surface:

$$\partial_r u(t,r=R_h^+)=-\frac{\dot{p}_h(t)}{\gamma_s p_h(t)}-2\frac{\dot{R}_h}{R_h}. \tag{31}$$

Much more information can be obtained. For instance, by considering the momentum conservation equation in the vicinity of $r=R_h(t)^+$, we get

$$\ddot{R}_h(t)=\frac{d}{dt}u(t,R_h(t))=\partial_t u+\dot{R}_h\partial_r u=(\dot{R}_h-u(t,R_h(t)))\ \partial_r u-\frac{1}{\rho}\partial_r p\bigg|_{r=R_h^+},$$

which yields the pressure gradient

$$\partial_r p(t,r=R_h^+)=-\rho_{\rm sh}(t)\ddot{R}_h(t). \tag{32}$$

By substituting typical values for the acceleration, shell density, and pressure (see the next paragraph), we can check that the isobaric approximation in the shell is not fulfilled in general.

C. Dynamics of the baseline LMJ direct drive target

We now compare the predictions of our 1D model to 1D numerical simulations of the baseline LMJ direct-drive target.[12] The deceleration stage begins at time $t=12.1$ ns and lasts for about 450 ps. During this phase the target velocity changes from 400 km/s to 0 in less than 500 ps, which leads to deceleration as high as about 5000 μm/ns^2. In the same time, the ablation velocity of the shell inner layer increases to up to 32 μm/ns^{-1}. The density gradient scale length is about $L_{\rm min}\simeq 1$ μm. The Froude number increases to 0.4 at $t=12.3$ ns and decreases afterwards.

1D numerical simulations supply a full set of data at the beginning of the deceleration phase as initial conditions for our theoretical model such as (cf. Fig. 1):

$p_0=0.15$ Gbar (initial hot spot pressure),

$R_0=210$ μm (initial hot spot radius),

$\Delta_0=100$ μm (initial shell thickness),

$M_{\rm sh}=1.05$ mg (initial shell mass),

$M_{h0}=8$ μg (initial hot spot mass).

The value of the initial hot spot mass M_{h0} is only used in Eq. (28) for the determination of the hot spot mass during the

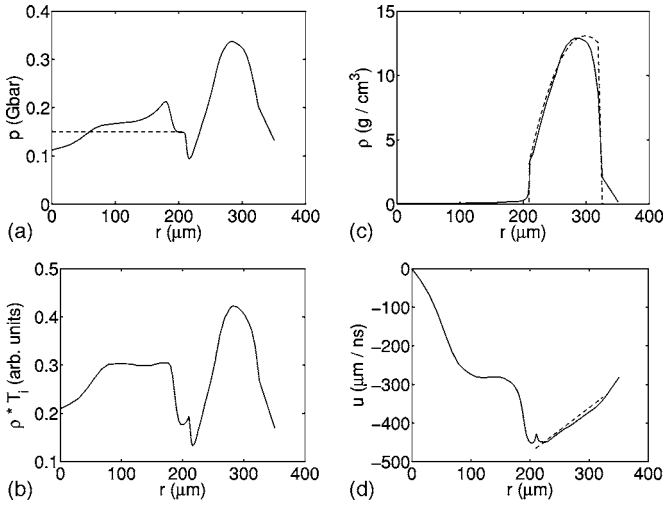

FIG. 1. Initial conditions corresponding to the output data of a numerical simulation of the acceleration phase (solid lines): pressure (a), product ρT_i (proportional to the pressure for an ideal gas) (b), density (c), and velocity (d). The dashed lines correspond to the interpolations used for the theoretical model.

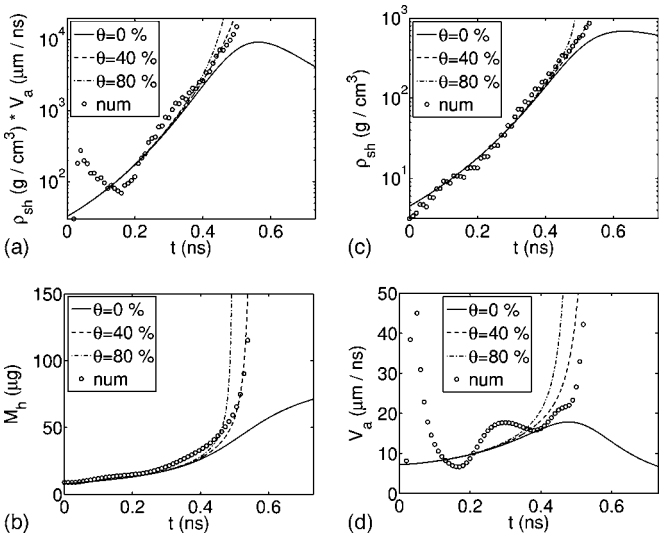

FIG. 3. Time evolutions of the mass flow (a), hot spot mass (b), shell density (c), and ablation velocity (d).

deceleration phase. The initial density profile is approximated by a quadratic function [Fig. 1(c)]. The initial velocity profile is approximated by the linear function (15) with $V_i = 465\ \mu$m/ns and $\eta_0 = 0.25$ [Fig. 1(d)].

The system of five differential equations (23)–(27) has been integrated with the above initial conditions and we report in Figs. 2–4 the time evolutions of the physically relevant quantities. The values for the physical parameters are $\nu = 5/2$, $c_v = 10^4\ \mathrm{m^2\ s^{-2}\ K^{-1}}$, $\chi = 6\times 10^{-8}\ \mathrm{m\ g\ s^{-3}\ K^{-7/2}}$, $\gamma_h = 5/3$, $\gamma_s = 7/4$, and $\mu_\alpha = \theta\ 9.12\times 10^{-10}\ \mathrm{m\ s\ g^{-1}}$, where θ is the absorbed α-particle fraction. The case $\theta = 0$ corresponds to the absence of nuclear reaction. The cases $\theta = 40\%$ and 80% take into account fusion reactions. Time 0 is the beginning of the deceleration phase. The predictions of the theoretical model (lines) are compared to the results from full numerical simulations (circles), which shows excellent agreement. Only the prediction of the central hot spot density [Fig. 4(a)] exhibits a noticeable discrepancy (25%). This may be connected with the fact that the numerical code is flux-limited, so that the conductivity law used in the numerical code is not a Spitzer law with exponent $\nu = 5/2$. This has a dramatic influence of the shape factor m_ν given by (29) and this may be the origin of the observed departure. By applying an ad-hoc corrective factor [Fig. 4(b)], a very good agreement is restored.

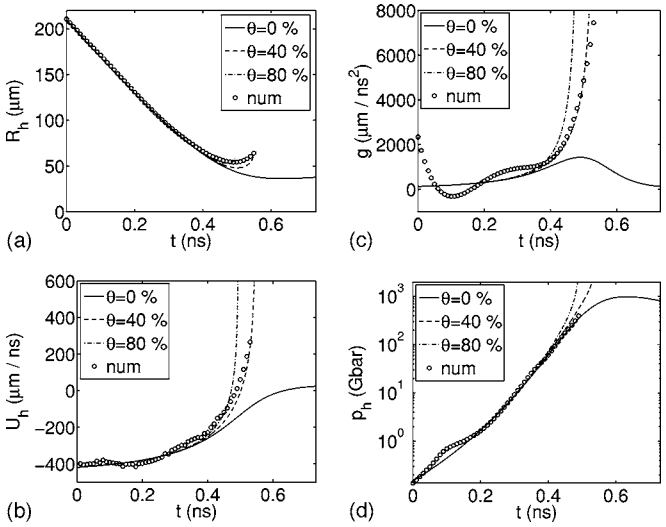

FIG. 2. Time evolutions of the hot spot radius (a), velocity (b), acceleration (c), and pressure (d). Circles correspond to the numerical simulations.

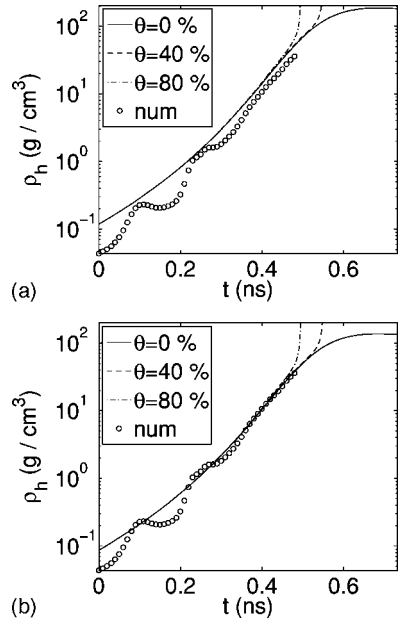

FIG. 4. Time evolution of the central hot spot density. (a) The numerical results (circles) and the predictions of the theoretical model with $\nu = 5/2$. A departure of 25% is noticeable. In (b) a corrective factor of 0.75 has been applied to the theoretical predictions, which gives a very good agreement.

III. THE RAYLEIGH-TAYLOR INSTABILITY IN A NON-STEADY STATE REGIME

A. Linear stability analysis

The object of the following is to develop an analytical model to describe the temporal evolution of the weakly two-dimensional perturbations, particularly the amplitude ξ_l of the perturbed inner shell surface (boundary of the hot spot), where l is the Legendre index of the spherical harmonics $Y_l^m(\theta,\phi)$; θ and ϕ are the polar and azimuthal angles, respectively. An ablation front separates the hot spot from the shocked shell region, and we develop a model that takes into account the following physical effects: compressibility of the shell, ablation at the inner shell surface, and, consequently, the damping effect of both the vorticity-convection off the ablation front and fire polishing. The most important result of this section is the (differential) equation that describes the temporal evolution of the small perturbations in the linear stability analysis. The study of the perturbations in the hot spot is based on the one-dimensional self-similar solution described in Sec. II. This solution is perturbed and an exact linear analysis (not carried out in Refs. 5 and 6) is performed. The effect of compressibility in the shocked shell is taken into account in a crude but treatable way, by considering a uniform shell density that varies arbitrarily in time, $\rho_{\rm sh}(t)$, and by introducing the velocity potential ϕ such that $\mathbf{u}=\nabla\phi$, leading to a continuity equation of the form $\Delta\phi=-\partial_t \ln \rho_{\rm sh}$, and to a momentum equation giving us the Bernoulli equation. This approximation has already been applied successfully in the past by several authors.[16–20]

1. Shocked shell analysis ($r>R_h$)

The shocked shell region is simplified to a region of uniform density, but varying arbitrarily in time, $\rho_{\rm sh}(t)$, and following the analysis of Refs. 17 and 20 we introduce the velocity potential ϕ leading to a continuity equation of the form

$$\Delta\phi = -\partial_t \ln \rho_{\rm sh}. \tag{33}$$

The solution for the potential $\phi=\phi_0+\phi_1$, retaining only those perturbations that decrease away from the interface, is

$$\phi_0 = A_0 + \frac{B_0}{r} - \frac{r^2}{6}\partial_t \ln \rho_{\rm sh},$$

$$\phi_1 = \sum_{l,m} \frac{B_l^m}{r^{l+1}} Y_l^m(\theta,\phi),$$

where the coefficients A_0, B_0, and B_l^m are functions of time to be determined. The momentum equation for the velocity potential gives the Bernoulli equation:

$$\partial_t\phi + \frac{1}{2}|\nabla\phi|^2 + \frac{p_0+p_1}{\rho_{\rm sh}} = 0, \tag{34}$$

where p_0 and p_1 are the unperturbed and perturbed pressure, respectively, and the flow mass conservation through the shell inner surface gives us

$$\nabla\phi\cdot\ \mathbf{n}|_{\rm inn} = \mathbf{n}\cdot\mathbf{e}_r\partial_t\, r_{\rm sh}|_{\rm inn} + \frac{\dot m}{\rho_{\rm sh}}. \tag{35}$$

Here $\mathbf{e}_r$, $\mathbf{e}_\theta$, and $\mathbf{e}_\phi$ are the usual unit vectors in spherical coordinates. Let

$$r_{\rm sh} = R_h(t) + \sum_{l,m} \xi_l^m(t) Y_l^m(\theta,\phi) \tag{36}$$

be the perturbed position of the inner surface. The mass flow rate $\dot m$ relative to this interface (toward the inner region with normal unit vector $\mathbf{n}$) is by definition:

$$\dot m = \dot m_0(t) + \sum_{l,m} \dot m_{1l}^m(t) Y_l^m(\theta,\phi)$$
$$= \rho_{\rm sh}(t)(\mathbf{u}\cdot\mathbf{n} - \mathbf{e}_r\cdot\mathbf{n}\partial_t r_{\rm sh})_{\mathbf{r}=(r_{\rm sh},\theta,\phi)}. \tag{37}$$

The momentum flux Q relative to the shell inner surface toward the inner region is

$$Q = Q_0(t) + \sum_{l,m} Q_{1l}^m(t) Y_l^m(\theta,\phi) = \frac{\dot m^2}{\rho_{\rm sh}} + p\Big|_{\mathbf{r}=(r_{\rm sh},\theta,\phi)}. \tag{38}$$

Now, linearizing Eqs. (34)–(38) in ξ_l^m and eliminating B_0 and B_l^m, we get the following ordinary differential equation for the modal amplitude:

$$\ddot\xi_l^m + \left[\frac{(l-1)V_a}{R_h} + 3\frac{\dot R_h}{R_h} + \frac{\dot\rho_{\rm sh}}{\rho_{\rm sh}}\right]\dot\xi_l^m$$
$$- \left[(l-1)\frac{\ddot R_h - \dot V_a}{R_h} - \frac{\ddot\rho_{\rm sh}}{\rho_{\rm sh}} + \frac{\dot\rho_{\rm sh}^2}{\rho_{\rm sh}^2} - \frac{\dot R_h\dot\rho_{\rm sh}}{R_h\rho_{\rm sh}}\right]\xi_l^m$$
$$= Q_{1l}^m\frac{l+1}{R_h\rho_{\rm sh}} + \partial_t\left(\frac{\dot m_{1l}^m}{\rho_{\rm sh}}\right) + \frac{\dot R_h - V_a(l+1)}{R_h}\frac{\dot m_{1l}^m}{\rho_{\rm sh}}, \tag{39}$$

where $V_a=\dot m_0/\rho_{\rm sh}$ represents the ablation velocity. Equation (39) gives us the temporal evolution of the perturbed interface if the right-hand side (Q_{1l}^m and $\dot m_{1l}^m$) is fixed. The analysis of the hot region will allow us to obtain Q_{1l}^m and $\dot m_{1l}^m$. For a passive interface, with $Q_{1l}^m=0$, $\dot m_{1l}^m=0$, and $V_a=0$, Eq. (39) reproduces the well-known Bell-Plesset equation of convergent flows.[21]

Finally, the tangential velocity $\mathbf{u}_\tau$ is also conserved through the interface, or equivalently up to the linear order in the perturbed amplitude $\nabla_\perp\cdot\mathbf{u}_\tau=(\sin\theta)^{-1}(\partial_\theta(\sin\theta u_\theta)+\partial_\phi u_\phi)$. After some algebra and writing $\nabla_\perp\cdot\mathbf{u}_\tau=\Sigma_{l,m}(\nabla_\perp\cdot\mathbf{u}_\tau)_l^m Y_l^m$, we get

$$(\nabla_\perp\cdot\mathbf{u}_\tau)_l^m = -l\left(\frac{\dot m_{1l}^m}{\rho_{\rm sh}} + \left(2\frac{V_a-\dot R_h}{R_h} - \frac{\dot\rho_{\rm sh}}{\rho_{\rm sh}}\right)\xi_l^m - \dot\xi_l^m\right). \tag{40}$$

2. Hot spot region $r<R_h$

The system of equations (1)–(6) is used to determine the flow in the hot spot when it is perturbed with respect to the self-similar solution. The analysis of perturbations is troublesome and such a difficulty is mainly based on the fact that the unperturbed flow solution is singular at $r=R_h$. To carry out the analytical-numerical study it is convenient to use the following variables:

$$\eta = \frac{r}{r_{\rm sh}} \simeq \frac{r}{R_h(t)}\left[1 - \sum_{l,m} \xi_l^m(t) Y_l^m(\theta,\phi)\right],$$

$$T^\nu = T_h(t)^\nu \left[\psi_0(\eta) + \sum_{l,m} \psi_{1l}^m(\eta,t) Y_l^m(\theta,\phi)\right],$$

$$\mathbf{u} = \left[u_0(t,\eta) + \sum_{l,m} u_{1l}^m(t,\eta) Y_l^m(\theta,\phi)\right]\mathbf{e}_r + \mathbf{u}_\perp,$$

$$\nabla_\perp \cdot \mathbf{u}_\perp = \sum_{l,m} w_{1l}^m(t,\eta) Y_l^m(\theta,\phi),$$

$$p = p_0 + \sum_{l,m} p_{1l}^m(t,\eta) Y_l^m(\theta,\phi).$$

The rotational component of the velocity can also be expanded as

$$\mathbf{u}_{\rm rot} = \left[\sum_{l,m} (u_{{\rm rot},1l}^m(t,\eta) + r\partial_t(\xi_l^m/R_h)) Y_l^m(\theta,\phi)\right]\mathbf{e}_r + \mathbf{u}_{{\rm rot},\perp},$$

$$\nabla_\perp \cdot \mathbf{u}_{{\rm rot},\perp} = \sum_{l,m} w_{{\rm rot},1l}^m(t,\eta) Y_l^m(\theta,\phi).$$

Using (5), the linear perturbations u_1, $u_{{\rm rot},1}$, w_1, and $w_{{\rm rot},1}$ satisfy

$$u_{1l}^m = a_\nu V_b \psi_0^{1/\nu}\left(\partial_\eta \psi_{1l}^m + \left(\frac{\psi_{1l}^m}{\nu\psi_0} - \frac{\xi_l^m}{R_h}\right)\partial_\eta\psi_0\right) + \eta\dot{\xi}_l^m + u_{{\rm rot},1l}^m,$$

$$w_{1l}^m = a_\nu V_b l(l+1)\psi_0^{1/\nu}\left(\frac{\xi_l^m}{R_h}\eta\partial_\eta\psi_0 - \psi_{1l}^m\right) + w_{{\rm rot},1l}^m.$$

We substitute these expressions into the system of equations (1)–(6). Collecting the zero-order terms we get the system studied in the previous sections giving the self-similar solution. Collecting the first-order terms we get a fifth-order differential system for the linear perturbations:

$$\frac{(R_h/V_b)\partial_t\psi_{1l}^m - \psi_{1l}^m - (u_{{\rm rot},1l}^m/V_b)\partial_\eta\psi_0}{\nu\psi_0^{1/\nu}} + \frac{a_\nu}{\eta^2}\partial_\eta(\eta^2\partial_\eta\psi_{1l}^m) - \frac{l(l+1)a_\nu}{\eta^2}\psi_{1l}^m + \frac{2\xi_l^m}{R_h\psi_0^{1/\nu}} + \frac{l(l+1)\xi_l^m}{R_h\eta}a_\nu\partial_\eta\psi_0 = 0, \tag{41}$$

$$\frac{\rho_h}{\psi_0^{1/\nu}}\left[\partial_t u_{1l}^m + \left(\frac{u_0}{R_h} - \eta\frac{\dot{R}_h}{R_h}\right)\partial_\eta u_{1l}^m + \frac{u_{1l}^m}{R_h}\partial_\eta u_0 - \left(\eta\partial_t\left(\frac{\xi_l^m}{R_h}\right) + \frac{\xi_l^m u_0}{R_h^2}\right)\partial_\eta u_0\right] = -\frac{1}{R_h}\partial_\eta p_{1l}^m + \left(\frac{\xi_l^m}{R_h^2} - \frac{\psi_{1l}^m}{\nu\psi_0}\frac{1}{R_h}\right)\partial_\eta p_0, \tag{42}$$

$$\frac{\rho_h}{\psi_0^{1/\nu}}\left[\partial_t w_{1l}^m + \left(\frac{u_0}{R_h} - \eta\frac{\dot{R}_h}{R_h}\right)\partial_\eta w_{1l}^m + \frac{u_0 w_{1l}^m}{R_h\eta}\right] = \frac{l(l+1)}{R_h\eta}\left(p_{1l}^m - \frac{\xi_l^m}{R_h}\eta\partial_\eta p_0\right), \tag{43}$$

$$\frac{\partial_\eta(\eta^2 u_{{\rm rot},1l}^m)}{\eta} + w_{{\rm rot},1l}^m = -3\eta R_h\partial_t\left(\frac{\xi_l^m}{R_h}\right). \tag{44}$$

The variables ψ_{1l}^m, $u_{{\rm rot},1l}^m$, $w_{{\rm rot},1l}^m$, and p_{1l}^m, must also verify the following boundary conditions.

(a) At the ablation front $\eta\to 1^-$, the perturbed temperature must vanish

$$\psi_{1l}^m(t,\eta=1^-) = 0. \tag{45}$$

(b) The perturbed mass flow rate and momentum flux along the normal direction to the ablation front must be bounded. It is possible to show that this condition means that $u_{{\rm rot},1l}^m$ must vanish at $\eta=1^-$. Indeed, the perturbed mass flow rate is $\dot{m}_{1l}^m/(\rho_h V_b) = -a_\nu\partial_\eta\psi_{1l}^m + \xi_l^m a_\nu\partial_\eta\psi_0 + u_{{\rm rot},1l}^m/(V_b\psi_0^{1/\nu})$. Since $\psi_0(\eta)\to 0$ as $\eta\to 1$, $u_{{\rm rot},1l}^m$ must vanish:

$$u_{{\rm rot},1l}^m(t,\eta=1^-) = 0. \tag{46}$$

Furthermore, using (44), $u_{{\rm rot},1l}^m \sim 1-\eta$ as $\eta\to 1$, so that $u_{{\rm rot},1l}^m/\psi_0^{1/\nu} \sim (1-\eta)^{1-1/\nu}\to 0$ as $\eta\to 1$, and the perturbed mass flow is

$$\frac{\dot{m}_{1l}^m}{(\rho_h V_b)} = -a_\nu\partial_\eta\psi_{1l}^m(t,\eta=1^-) + \xi_l^m a_\nu\partial_\eta\psi_0(\eta=1^-). \tag{47}$$

And similarly for the momentum flux, which contains only the perturbed pressure at the ablation front:

$$p_{1l}^m(t,\eta=1^-) = Q_{1l}^m. \tag{48}$$

Note that the perturbed tangential velocity (the transverse divergence) at the ablation front is simplified to

$$w_{{\rm rot},1l}^m(t,\eta=1^-) = -l\left[\frac{\dot{m}_{1l}^m}{\rho_{\rm sh}} + \xi_l^m\left(2\frac{V_a}{R_h} - 2\frac{\dot{R}_h}{R_h} - \frac{\dot{\rho}_{\rm sh}}{\rho_{\rm sh}}\right) - \dot{\xi}_l^m\right]. \tag{49}$$

(c) Variables must be bounded at $\eta=0$. It is possible to show that there are two unbounded modes.

The fifth-order partial differential system with the seven boundary conditions contained in (a), (b), and (c) gives us the solution together with the two eigenvalues $\dot{m}_{1l}^m$ and Q_{1l}^m. In order to solve that system, it is assumed that $V_b(t) \gg \dot{R}_h$ in the velocity expression, as in fact it is the case close to the stagnation time. Then the time derivatives are small compared with convective derivatives, $\partial_t \simeq \dot{R}_h/R_h \ll u_0\partial_r \simeq V_b/R_h$, and every perturbed variable $V_1 = (\psi_{1l}^m, \partial_\eta\psi_{1l}^m, u_{{\rm rot},1l}^m, w_{{\rm rot},1l}^m)$, or linear combinations of these variables, is expanded as $V_1 = V_1^1 + V_1^2 + \cdots$, with $|V_1^1| \gg |V_1^2| \gg \ldots$. The equations of the system (44) are also expanded, so that we obtain the following hierarchy of equations:

$$A_1\partial_\eta V_1^1 + B_1 V_1^1 = C_1\xi_l^m, \tag{50}$$

$$A_1\partial_\eta V_1^2 + B_1 V_1^2 = C_2\xi_l^m + C_2'\dot{\xi}_l^m + A_2\partial_t V_1^1 + B_2 V_1^1, \ldots, \tag{51}$$

where A_j, B_j, C_1, C_2, C_2' are matrix functions or vectors, depending on the zero-order solution. In particular the perturbed momentum flux and mass flow rate at the ablation front can be expanded as

$$\frac{Q_{1l}^m}{\dot{m}_0 V_b(\xi_l^m/R_h)} = q_1^1 + \frac{\dot{R}_h}{V_b} q_1^2 + \frac{R_h}{V_b}\frac{\dot{\rho}_{\rm sh}}{\rho_{\rm sh}} q_1^3 + \frac{R_h}{V_b}\frac{\dot{\xi}_l^m}{\xi_l^m} q_1^4 + \frac{R_h \dot{V}_b}{V_b^2} q_1^5 + \cdots, \tag{52}$$

$$\frac{\dot{m}_{1l}^m}{\dot{m}_0(\xi_l^m/R_h)} = f_1^1 + \frac{\dot{R}_h}{V_b} f_1^2 + \frac{R_h}{V_b}\frac{\dot{\rho}_{\rm sh}}{\rho_{\rm sh}} f_1^3 + \frac{R_h}{V_b}\frac{\dot{\xi}_l^m}{\xi_l^m} f_1^4 + \frac{R_h \dot{V}_b}{V_b^2} f_1^5 + \cdots, \tag{53}$$

where q_1^j, f_1^j are functions of the Legendre index l, and q_1^1, f_1^1 represent the leading order terms of the expansion. The other perturbed variables are expanded in a similar way. The hierarchy of equations (50) and (51) and boundary conditions (a), (b), and (c), give us the solution and the eigenvalues $q_1^j(l), f_1^j(l)$. Finally, using Eqs. (52) and (53) in Eq. (39), and neglecting $\rho_0(0,t)/\rho_{\rm sh}(t)$ terms, we get the following differential equation for the modal amplitude ξ_l^m:

$$\ddot{\xi}_l^m + \dot{\xi}_l^m \left[\frac{V_a}{R_h}((l-1) - f_1^1 - (l+1)q_1^4) + 3\frac{\dot{R}_h}{R_h} + \frac{\dot{\rho}_{\rm sh}}{\rho_{\rm sh}} \right] - \xi_l^m \left[(l-1)\frac{\ddot{R}_h - \dot{V}_a}{R_h} + \frac{\dot{V}_a}{R_h} f_1^1 + (l+1)\frac{V_a}{R_h}\left(\frac{\dot{R}_h}{R_h} q_1^2 + \frac{\dot{\rho}_{\rm sh}}{\rho_{\rm sh}} q_1^3 \right) - \frac{\ddot{\rho}_{\rm sh}}{\rho_{\rm sh}} + \frac{\dot{\rho}_{\rm sh}^2}{\rho_{\rm sh}^2} - \frac{\dot{R}_h}{R_h}\frac{\dot{\rho}_{\rm sh}}{\rho_{\rm sh}} + 3(l+1)\frac{\rho_{\rm sh} V_a^2}{\bar{\rho}_h R_h^2} q_1^1 \right] = 0, \tag{54}$$

where $\bar{\rho}_h$ is the average density in the hot spot, given in terms of the central hot spot density by $\bar{\rho}_h(t) = -a_\nu \partial_\eta \psi_0(1^-)\rho_h(t)$ ($\simeq 1.75\rho_h(t)$ if $\nu = 5/2$). The decomposition of the velocity field into potential and rotational parts helps us to understand the physical mechanism of stabilization. The potential part (thermal effects) is directly responsible for the mass ablation at the ablation front, $\dot{m}_{1l}^m/(\rho_0(t,0)V_b) = -a_\nu \partial_\eta \psi_{1l}^m + \xi_l^m a_\nu \partial_\eta \psi_0$ (fire polishing effect) through the terms involving f_1^1 in Eq. (54). The rotational part of the velocity field (dynamic effect), terms involving q_1^j, produces the perturbed momentum flux or perturbed ablation pressure p_{1a}. Indeed, let us write the vorticity $\omega = \omega_r \mathbf{e}_r + \omega_\perp$ where $\omega_\perp$ is its transverse component, and let us expand $\nabla_\perp \cdot (\omega_\perp \times \mathbf{e}_r) = \Sigma_{l,m} \Omega_l^m Y_l^m$. It can then be shown that the following identity is verified:

$$\Omega_l^m = \partial_r w_{{\rm rot},1l}^m + \frac{w_{{\rm rot},1l}^m}{r} + \frac{l(l+1)}{r}\left(u_{{\rm rot},1l}^m + \dot{\xi}_l^m - \xi_l^m \frac{\dot{R}_h}{R_h} \right),$$

and taking into account the behaviors of $w_{{\rm rot},1l}^m$ and $u_{{\rm rot},1l}^m$ at $\eta = 1^-$, we get

$$-\frac{\Omega_l^m}{l(l+1)}(\eta = 1^-) = \frac{p_{1a}}{\dot{m}_0 R_h} \simeq q_1^1 \frac{V_b \xi_l^m}{R_h^2} + q_1^2 \frac{\dot{R}_h \xi_l^m}{R_h^2} + q_1^3 \frac{\dot{\rho}_{\rm sh} \xi_l^m}{\rho_{\rm sh} R_h} + q_1^4 \frac{\dot{\xi}_l^m}{R_h} + \cdots.$$

In Fig. 5(a), the negative-valued functions f_1^1, q_1^1, q_1^2, q_1^3, and q_1^4 are plotted versus the Legendre index l. They are required as parameters in the ordinary differential equation (54). In Fig. 5(b) the spatial profiles for the leading perturbed pressure, vorticity, and temperature are plotted for the mode $l = 8$. We can thus check that the spatial profiles are not exponentially decaying functions of the distance from the ablation front ($\eta = 1$), but their maxima can be located inside the hot spot. This involves a displacement of the maximum of the Lagrangian perturbation amplitude inside the hot spot and evolving in time, which has been observed in numerical simulations.[12]

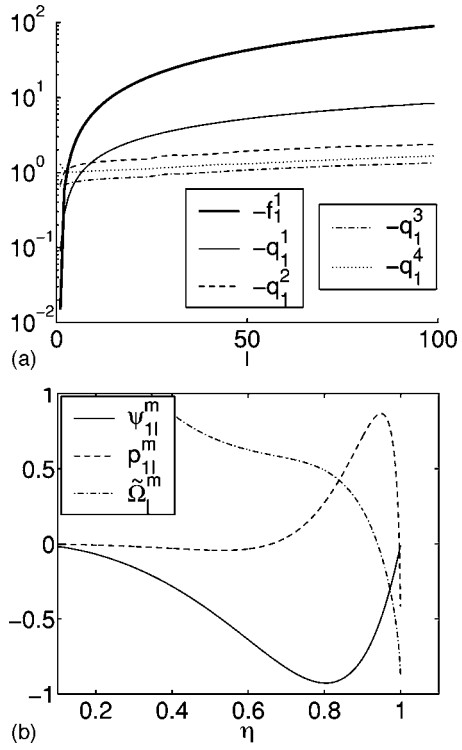

FIG. 5. (a) Functions f_1^1, q_1^1, q_1^2, q_1^3, and q_1^4 (multiplied by -1) vs the Legendre index l. (b) Normalized spatial profiles for the leading-order perturbed pressure p_{1l}^m, vorticity $\tilde{\Omega}_l^m := -\Omega_l^m R_h^2/[l(l+1)V_b \xi_l^m]$, and temperature ψ_{1l}^m for the mode $l = 8$.

B. Numerical simulations

For 2D single-mode calculations, we have used the hydrodynamics DUED code,[8–10] which includes radiative transfer, flux-limited electron conduction, atomic physics, real-matter equation of state,[22] and diffusion of fusion alpha-particles. The initial conditions for the 2D calculations were extracted from 1D data given by FCI2 simulations.[23]

1D hydrodynamics profiles are remapped onto a 2D perturbed mesh at the early deceleration time. The perturbation of the mesh is done along the radial direction by the quantity $\delta R(r,\theta,t=0) = \xi_l(r,t=0)P_l[\cos(\theta)]$, with l the mode number, P_l the Legendre polynomial, and θ the angle between the radial direction and the symmetry axis. Initially, the perturbation decreases exponentially along the radial direction according to $\xi_l(r,t=0) = \xi_{l0}\exp[-l|r/R_h(t=0) - 1|]$, where ξ_{l0} is the maximum initial amplitude located at the hot-spot radius R_h. A small maximum initial amplitude perturbation $\xi_{l0} = 10^{-3}$ μm has been chosen in order to remain always in the

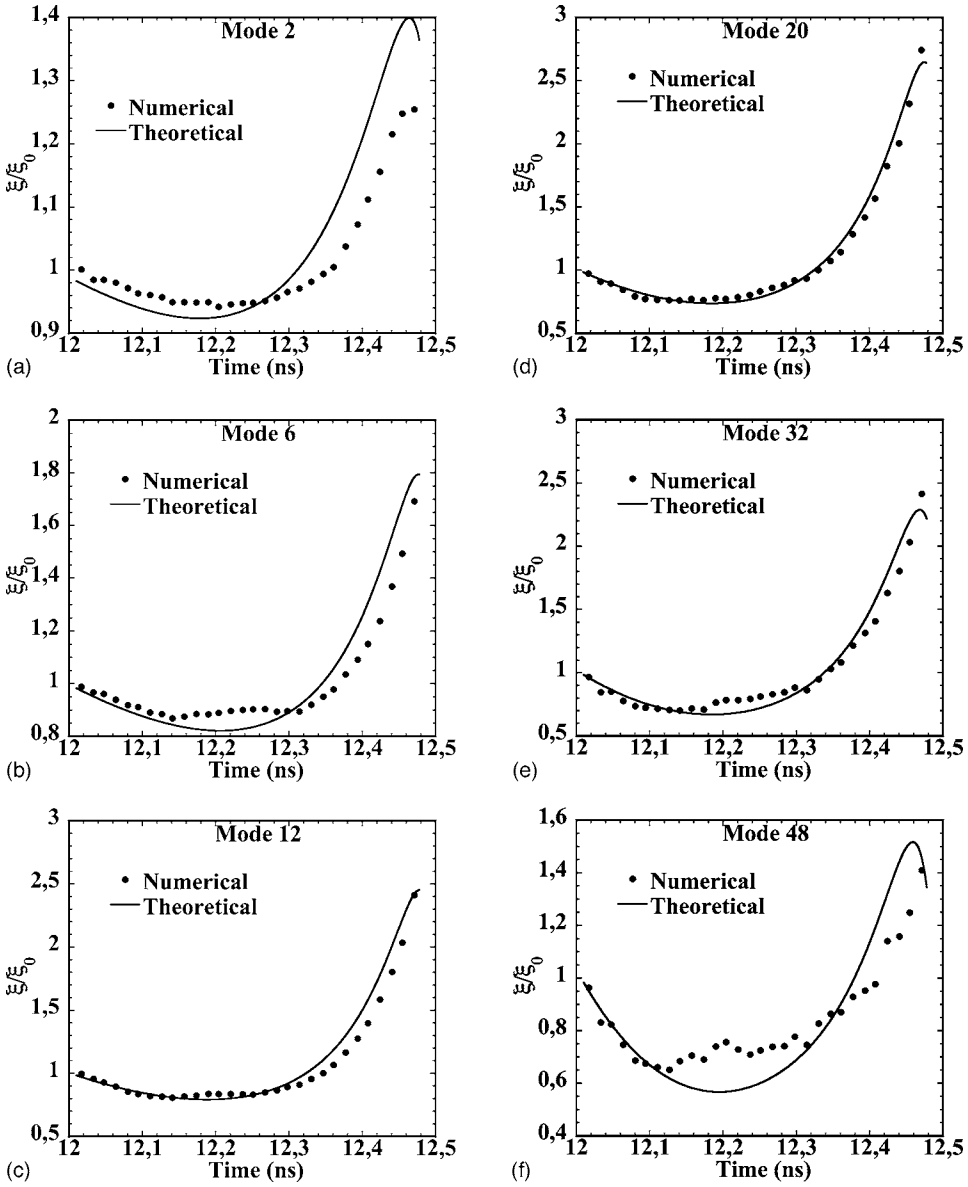

FIG. 6. Growths of the mode amplitudes vs time for different mode numbers l. The results of full numerical simulations (circles) are compared with the theoretical predictions (solid lines).

linear regime ($\xi_{l0} \ll k^{-1} = R_h/l$). The two-dimensional simulated domain covers a quarter of capsule. The calculations are driven until the stagnation time and the whole thermonuclear emission. Mode numbers between 2 and 64 have been simulated and the amplitudes of perturbation at the hot spot surface have been time resolved. The amplification of the mode amplitude becomes relevant at roughly 150 ps before the stagnation time. During this time interval, the instability remains always in its linear regime in the sense that non-initialized mode amplitudes are almost two orders of magnitude lower than the primary mode amplitude.

The theoretical model discussed in Sec. II is used to generate the unperturbed 1D flow. The linear stability analysis performed in Sec. III A can then be used to predict the RTI growth rates of this flow. According to formula (54), the acceleration, velocity, and position of the hot spot radius are required, as well as the ablation velocity, the shell density, and the central hot spot density. All these quantities can be obtained from our theoretical 1D model. As a consequence we can integrate the second-order ordinary differential equation (54) governing the growth of the amplitude $\xi_l(t)$ of the Legendre mode l. In order to integrate this differential equation, initial amplitude $\xi_l(0)$ and its time derivative $\dot{\xi}_l(0)$ are needed at the beginning. The way initial perturbation is implemented into DUED calculation imposes a non-zero value for $\dot{\xi}_l(0)$. This initial condition is a key parameter to match the solution $\xi_l(t)$ with numerical results.

We have checked that a variation of θ, the absorbed α-particle fraction, around 60% has no significant effect onto the total amplification of modes. Figure 6 shows the time evolution of $\xi_l(t)$ for low modes and high modes. A good agreement between numerical and theoretical results is achieved for intermediate modes which are the most amplified ones. Moreover, the numerical and theoretical time behaviors of low and high modes are similar except for modes beyond the cut-off wave number. These observations are the consequences of accounting for convergence effects, critical for low modes, and ablative stabilization important for high modes into our theoretical model.

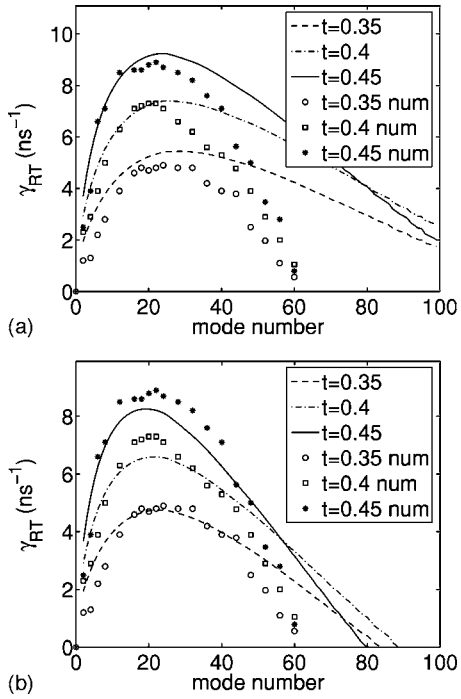

FIG. 7. Instantaneous growth rates of the mode amplitudes without the corrective factor for the central hot spot temperature (a) and with the corrective factor 0.75 (b).

The time derivatives of the logarithms of the mode amplitudes, which can be viewed as instantaneous growth rates,

$$\gamma_{RT}(l,t) = \frac{1}{\xi_l(t)} \frac{d\xi_l(t)}{dt},$$

are plotted in Fig. 7(a). The theoretical results obtained with the predicted one-dimensional flow are represented in solid lines. By comparing with the numerical results, we can observe that the ablative stabilization of high modes is underestimated by the model. We do believe that this is connected to the overestimation of the central hot spot density discussed in Sec. II, Fig. 4. If we apply the corrective factor 0.75 to the predicted central hot spot density, then the corrected density prediction is close to numerical density, and using this correction the predicted growth rates are also found in good agreement with the ones obtained from direct numerical simulations [cf. Fig. 7(b)]. A more physical way to compensate for the overestimation of the central hot spot temperature is to reduce the value of the Spitzer exponent which is taken to be equal to $\nu=5/2$ in the theoretical model, while the numerical scheme is flux-limited and cannot be fitted exactly by a Spitzer conductivity law.

IV. CONCLUSION

In this paper, we have presented a detailed 1D modeling and a self-consistent linear stability analysis of an ICF capsule during the decelerating stage. Taking into account the time dependence of the 1D flow is important as the unperturbed flow parameters vary in a stronger fashion than the perturbation amplitudes. The linear stability analysis is carried out on the exact self similar solution, which improves significantly the previous models based on the SBM approximation. In particular, the growth rates of low and intermediate modes are accurately predicted by the model, which shows that convergence effects and time dependence of the 1D flow are well captured. This is confirmed by numerical simulations of the baseline LMJ direct drive target, which also exhibit a slight discrepancy on the cutoff mode number, connected to an overestimation of the central hot-spot temperature. A tentative explanation is discussed in Sec. III B, and other mechanisms are under investigation. Work is also in progress about the combustion phase modeling in order to extend the application range beyond the ignition time.

ACKNOWLEDGMENTS

J.S. acknowledges the hospitality of the CEA-DIF and the support of the CICYT of Spain (FTN 2000-20048-C0301) and of the "Scretaria de Estado de Educacion y Universidades de Espana" (Programa de Sabaticos).

[1] V. Lobatchev and R. Betti, Phys. Rev. Lett. **85**, 4522 (2000).
[2] R. Betti, M. Umansky, V. Lobatchev, V. N. Goncharov, and R. L. McCrory, Phys. Plasmas **8**, 5257 (2001).
[3] R. Betti, K. Anderson, V. N. Goncharov, R. L. McCrory, D. D. Meyerhofer, S. Skupsky, and R. P. J. Town, Phys. Plasmas **9**, 2277 (2002).
[4] R. Betti, V. N. Goncharov, R. L. McCrory, and C. P. Verdon, Phys. Plasmas **5**, 1446 (1998).
[5] J. Garnier and C. Cherfils, Phys. Plasmas **12**, 012704 (2005).
[6] J. Sanz and R. Betti, Phys. Plasmas **12**, 042704 (2005).
[7] S. Atzeni and M. Temporal, Phys. Rev. E **67**, 1433 (2003).
[8] S. Atzeni, Comput. Phys. Commun. **43**, 107 (1986).
[9] S. Atzeni, Plasma Phys. Controlled Fusion **29**, 1535 (1987).
[10] S. Atzeni and M. L. Ciampi, Nucl. Fusion **37**, 1665 (1997).
[11] H. Takabe, L. Montierth, and R. L. Morse, Phys. Rev. A **38**, 1433 (1993).
[12] B. Canaud, X. Fortin, F. Garaude, C. Meyer, F. Philippe, M. Temporal, S. Atzeni, and A. Schiavi, Nucl. Fusion **44**, 1118 (2004).
[13] M. C. Herrmann, M. Tabak, and J. D. Lindl, Nucl. Fusion **41**, 99 (2001).
[14] Y. Saillard, in *Proceedings of Inertial Fusion Sciences and Applications 2001* (Elsevier, Paris, 2002), pp. 192–196.
[15] The SESAME database, Los Alamos National Laboratory, LA-UR-94-1451, 1994. See National Technical Information Service Document No. DE94011699. Copies may be ordered from the National Technical Information Service, Springfield, VA 22161.
[16] S. E. Bodner, Phys. Rev. Lett. **33**, 761 (1974).
[17] J. Sanz, Phys. Rev. Lett. **73**, 2700 (1994).
[18] A. R. Piriz, J. Sanz, and L. F. Ibanez, Phys. Plasmas **4**, 1117 (1997).
[19] V. N. Goncharov, Ph.D. thesis, University of Rochester, Rochester, 1998.
[20] V. N. Goncharov, P. McKenty, S. Skupsky, R. Betti, R. L. McCrory, and C. Cherfils-Clerouin, Phys. Plasmas **7**, 5118 (2000).
[21] M. S. Plesset, J. Appl. Phys. **25**, 96 (1954).
[22] S. Atzeni, A. Caruso, and V. A. Pais, Laser Part. Beams **4**, 393 (1986).
[23] E. Buresi, J. Coutant, R. Dautray *et al.*, Laser Part. Beams **4**, 531 (1986).